Probing anisotropic heat transport using time-domain thermoreflectance with offset laser spots

Joseph P. Feser, and David G. Cahill

View Online   Export Citation

ARTICLES YOU MAY BE INTERESTED IN

Analysis of heat flow in layered structures for time-domain thermoreflectance
Review of Scientific Instruments **75**, 5119 (2004); https://doi.org/10.1063/1.1819431

Pulse accumulation, radial heat conduction, and anisotropic thermal conductivity in pump-probe transient thermoreflectance
Review of Scientific Instruments **79**, 114902 (2008); https://doi.org/10.1063/1.3006335

Pump-probe measurements of the thermal conductivity tensor for materials lacking in-plane symmetry
Review of Scientific Instruments **85**, 104903 (2014); https://doi.org/10.1063/1.4897622

Probing anisotropic heat transport using time-domain thermoreflectance with offset laser spots

Joseph P. Feser[a)] and David G. Cahill

Department of Materials Science and Engineering, and Materials Research Laboratory, University of Illinois, Urbana, Illinois 61801, USA

An analytic solution is derived for the time-domain thermoreflectance signal that occurs using non-concentric pump and probe beams on multilayer anisotropic materials. When in-plane heat transport is negligible, the experimental signal is the same as for the concentric case. However, for samples where in-plane heat diffusion distances are comparable to the spot size, the signal is sensitive to in-plane heat transport. This sensitivity to in-plane transport can be exploited to measure the in-plane thermal conductivity. Examples with experimental data are given for thin-film Al and the in-plane thermal conductivity of pyrolytic graphite. © *2012 American Institute of Physics.* [http://dx.doi.org/10.1063/1.4757863]

I. MOTIVATION

Time domain thermoreflectance (TDTR) is a pump-probe technique that is used to measure the thermal properties of materials and interfaces. The technique accomplishes this by heating the surface of a material using a train of laser pulses (pump beam) and by monitoring the resulting temperature change through the reflectivity of the surface sampled using a time-delayed sensing beam. Furthermore, the train of pump pulses is modulated, which is used for lock-in detection of the thermoreflectance signal and generates useful pulse accumulation effects.[1,2] The physical implementation of our two-tint TDTR system and the data reduction for layered materials has been described previously.[2,3] TDTR has been applied to measure the properties of a wide range of thin-films,[4] multilayers,[5] bulk materials, and their interfaces.[6]

Schmidt extended TDTR modeling to include multilayers with radial anisotropy.[1] By conducting experiments at multiple modulation frequencies, Schmidt demonstrated the ability of TDTR to measure the in-plane thermal conductivity of bulk materials[1] and thin-film metallic layers.[7]

Here, we present an alternative method for measuring the in-plane properties of materials based on sensing the surface temperature at a different lateral location than where the heat is introduced. A similar technique has been used for MEMS-based measurements of in-plane thermal conductivity,[8] but by using a pump-probe laser technique, our method avoids the need for microfabrication, and allows the offset distance between the heating and sensing regions to be varied continuously. Li[9] has described a similar optical technique and analysis based on thermoreflectance microscopy that is capable of measuring anisotropic thermal diffusivity of bulk samples. Our work extends this to time-domain thermoreflectance, and is based on a more general multilayer analysis. Schmidt has previously described a method for calculating the time-domain thermoreflectance signal,[1] whereby the spatial surface temperature distribution is explicitly calculated and then averaged with respect to a probe intensity distribution. Since the method requires numerical triple-integration, it is relatively computationally expensive. This work will show an alternative method of performing the calculation that is much faster and facilitates rapid interpretation of data.

First, an analytic model is derived for the TDTR signal obtained from using independent and arbitrarily-shaped laser beams with cylindrical symmetry to measure a material stack with an arbitrary number of layers/interfaces. The model is then extended to the case of non-concentrically aligned Gaussian beams, which is more easily experimentally accessed. The implications of the model to in-plane transport are discussed, and we show that when lateral diffusion is comparable to the laser spot-size, the signal obtained with non-concentric alignment can be used to measure the in-plane thermal conductivity of materials.

II. FREQUENCY DOMAIN SOLUTION FOR SURFACE TEMPERATURE PROBED USING AN OFFSET BEAM

When temperature fluctuations are small such that the heat transport equations are linear and time-invariant, the thermoreflectance signal measured during a TDTR experiment can be written in terms of the frequency-domain response of the thermal system:[2]

$$\text{Re}[\Delta R_M(t_d)] = \frac{dR}{dT} \sum_{m=-\infty}^{\infty} (\Delta T(mf_{\text{rep}} + f_{\text{mod}}) + \Delta T(mf_{\text{rep}} - f_{\text{mod}})) \exp(im2\pi f_{\text{rep}} t_d), \quad (1)$$

$$\text{Im}[\Delta R_M(t_d)] = -i\frac{dR}{dT} \sum_{m=-\infty}^{\infty} (\Delta T(mf_{\text{rep}} + f_{\text{mod}}) - \Delta T(mf_{\text{rep}} - f_{\text{mod}})) \exp(im2\pi f_{\text{rep}} t_d), \quad (2)$$

where f_{rep}, f_{mod}, and t_d are the laser repetition rate (in Hz), modulation frequency, and time delay, respectively. The frequency-domain response $\Delta T(f)$ is defined as the average temperature sampled by the sensing beam, due to a

---

continuous pump beam that is modulated sinusoidally in time at frequency f. In the case of systems where the mechanical stage advances the arrival time of the pump beam rather than delaying the probe, there is an additional phase factor $\Delta R(t_d) = \Delta R_M(t_d)\exp(i2\pi f_{\mathrm{mod}} t_d)$.

We have previously described the frequency domain solution to the temperature fluctuation detected by a Gaussian sensing beam concentrically aligned with a Gaussian pumping beam.[2] More generally, if the pumping and sensing beams are axisymmetric and concentrically aligned with intensity profiles $p(r)$ and $s(r)$, and the properties of a material stack are isotropic to in-plane transport (i.e., transport can be described in terms of only radial and through-plane thermal conductivities), then the temperature fluctuation detected by the sensing beam is given by

$$\Delta T(f) = \frac{2\pi}{A_S} \int_0^\infty G(f,k)P(k)S(k)k\,dk, \qquad (3)$$

where $P(k)$ and $S(k)$ are the Hankel transforms of the intensity profiles, and A_S is the total intensity of the sensing beam. Here, the Hankel transform is defined as

$$F(k) \equiv 2\pi \int_0^\infty f(r)J_0(2\pi kr)r\,dr. \qquad (4)$$

$G(f,k)$ is the Hankel transform of the Green's function solution for the temperature response due to a sinusoidally oscillating point source of unit strength. Cahill has described the methodology for computing $G(f,k)$ in cylindrical systems,[2] and Schmidt has extended this to include radially anisotropic layers.[1] The result is that $G(f,k)$ is obtained through an iterative procedure; numbering the layers from $n = 1$ for the layer that terminates the surface of the solid, and beginning the algorithm from the furthermost layer,

$$\begin{pmatrix} B^+ \\ B^- \end{pmatrix}_n = \frac{1}{2\gamma_n} \begin{pmatrix} \exp(-u_n L_n) & 0 \\ 0 & \exp(-u_n L_n) \end{pmatrix}$$

$$\times \begin{pmatrix} \gamma_n + \gamma_{n+1} & \gamma_n - \gamma_{n+1} \\ \gamma_n - \gamma_{n+1} & \gamma_n + \gamma_{n+1} \end{pmatrix} \begin{pmatrix} B^+ \\ B^- \end{pmatrix}_{n+1}, \qquad (5)$$

$$u_n \equiv \left[4\pi^2 k^2 \left(\frac{\kappa_r}{\kappa_z} \right) + q_n^2 \right]^{1/2}, \qquad (6)$$

$$q_n^2 \equiv \frac{i2\pi f}{D_n}, \qquad (7)$$

$$\gamma_n \equiv \kappa_{z,n} u_n, \qquad (8)$$

where each layer is described by the parameters, κ_r (radial thermal conductivity), κ_z (through-plane thermal conductivity), D (through-plane thermal diffusivity), and L (thickness).

$$G(f,k) = \left(\frac{B_1^+ + B_1^-}{B_1^+ - B_1^-} \right) \frac{1}{\gamma_1}. \qquad (9)$$

Note that when there is no radial heat transport in any of the layers (i.e., $\kappa_{r,n} = 0$), the transfer function becomes independent of k, which only enters into the determination of $G(f,k)$ through equation (6).
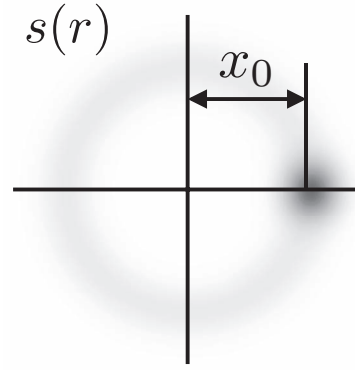

FIG. 1. Overlay of two equivalent intensity profiles for the sensing beam, $s(r)$. Sensing with an offset Gaussian beam (dark spot) is equivalent to redistributing the intensity evenly over a ring shaped object given by Eq. (12) (light ring). The pump beam is centered at the origin.

In order to obtain the frequency domain solution, what remains is to calculate the Hankel transforms $P(k)$ and $S(k)$. Note that the frequency domain solution (Eq. (3)), and thus the TDTR signal, is invariant upon exchanging the shape or intensity of the pumping and sensing beams.

The case of modeling two offset Gaussian pumping/sensing beams might appear not to fit into the Hankel transform framework used in Eq. (3), because the problem is not axisymmetric. However, the problem can be recast into a solvable one (Figure 1) by recognizing that sensing with an offset beam with intensity given by

$$s(x,y) = \frac{2A_S}{\pi w_S^2} \exp\left(-\frac{2[(x-x_0)^2 + y^2]}{w_S^2} \right), \qquad (10)$$

is equivalent to sensing with the ring-shaped axisymmetric profile,

$$s(r) = \frac{1}{2\pi} \int_0^\infty \frac{A_S}{\pi w_S^2}$$

$$\times \exp\left(\frac{-2[(r\cos\theta - x_0)^2 + (r\sin\theta)^2]}{w_S^2} \right) d\theta. \qquad (11)$$

Equation (11) can be integrated directly and yields

$$s(r) = \left(\frac{2A_S}{\pi w_S^2} \right) \exp\left(-\frac{2(r^2 + x_0^2)}{w_S^2} \right) I_0\left(\frac{4x_0 r}{w_S^2} \right), \qquad (12)$$

where I_0 is the zeroth-order modified Bessel function of the first kind. The Hankel transform of Eq. (12) can be derived as a series solution, using the Taylor expansion for I_0,

$$s(r) = \frac{2A_S}{\pi w_S^2} \exp\left(-2(r^2 + x_0^2) \right) \sum_{i=0}^\infty \frac{1}{n!} \left[\frac{4x_0^2 r^2}{w_S^4} \right]^n. \qquad (13)$$

The Hankel transform of Eq. (13) can obtained using the identity,

$$H(r^2 f(r)) = -\frac{1}{4\pi k} \frac{d}{dk}\left(k \frac{dF(k)}{dk} \right), \qquad (14)$$

which leads to the final result for $S(k)$.

$$S(k) = \frac{A_S}{\pi} \exp\left(-\left[\left(\frac{\sqrt{2}x_0}{w_S}\right)^2 + \left(\frac{\pi w_S k}{\sqrt{2}}\right)^2\right]\right)$$

$$\times \sum_{n=0}^{\infty} \frac{1}{(n!)^2} \left(\frac{\sqrt{2}x_0}{w_S}\right)^{2n} \ell_n\left(\frac{w_S k}{2}\right). \quad (15)$$

The polynomial $\ell(x)$ is defined recursively by

$$\ell_{n+1}(x) = -\frac{1}{k}\left[(\pi^2 x^3 - x)\ell_n(x) + \left(\frac{1}{4\pi^2} - x^2\right)\ell'_n(x)\right.$$

$$\left. + \frac{x}{4\pi^2}\ell''_n(x)\right], \quad (16)$$

where the first term of the polynomial is given by $\ell_0 = \pi$. Together, Eqs. (15) and (16) define the Hankel transform of the sensing beam. We find that the first 40 terms of the summation in Eq. (15) are sufficient to calculate the Hankel transform for $x_0 \leq 4w_0$. The pump beam is assumed to be Gaussian with total absorbed intensity, A_P, and centered at the origin so that its Hankel transform is given by

$$P(k) = A_P \exp\left(-\pi^2 k^2 w_P^2 / 2\right). \quad (17)$$

Thus, the Hankel Transforms $S(k)$, $P(k)$, and $G(f, k)$ can be evaluated and used to obtain the frequency domain response, $\Delta T(f)$, with Eq. (3), and the TDTR signal can then be evaluated using Eqs. (1) and (2).

Schmidt has previously reported a method to calculate the frequency domain response due to an offset laser spot.[1] Our approach is faster to evaluate numerically because the solution involves only a single integral in Hankel coordinates (Eq. (3)), whereas the solution in Ref. 1 involves a triple integral making it less efficient as a tool for data reduction. We have verified numerically that the solution given here yields identical results to Ref 1, but that the current model can be evaluated ~50 times faster.

Note that in the case of concentrically aligned beams ($x_0 = 0$), the Hankel transform of the sensing beam (Eq. (15)) reduces to

$$S(k) = A_S \exp\left[-\frac{\pi^2 w_s^2 k^2}{2}\right], \quad (18)$$

which recovers the expression derived previously in the case of conventional TDTR.[2]

$$\Delta T(f) = 2\pi A_P \int_0^{\infty} G(f, k) \exp\left[-\frac{\pi^2\left(w_s^2 + w_p^2\right)k^2}{2}\right] k\,dk. \quad (19)$$

III. THE EFFECT OF IN-PLANE TRANSPORT PROPERTIES ON EXPERIMENTAL SIGNALS

A. Experimental details

Using the results from Sec. II, we now examine the effect of in-plane properties on the experimental signal generated by non-concentrically aligned beams. The signal that is analyzed in TDTR is the ratio of the in-phase

voltage and out-of-phase voltage corresponding to the surface reflectivity oscillations at the modulation frequency, $\phi \equiv -V_{in}(t_d)/V_{out}(t_d) = -\text{Re}(\Delta R(t_d))/\text{Im}(\Delta R(t_d))$, which is chosen because it is independent of laser intensities, sample absorptivity, and thermoreflectance coefficient; hereafter, this will be referred to as "the ratio." For the experiments described in Subsections III B and III C, the ratio is studied as a function of the beam offset distance, x_0, at a fixed time delay, which will be referred to as a "beam offset sweep."

We produce controlled beam offset distances with a precision 2-axis goniometer (Newport model SL8ABD), which holds a polarizing beam splitter that serves to recombine the pump and probe beam after the delay stage and just before the microscope objective lens.[3] The goniometer is used to independently control the angle of the pump beam as it enters the microscope objective; a deviation in the entrance angle causes a beam offset on the sample, $\Delta x_0 = F\Delta\theta$, with $F = 200$ mm/M where M is the microscope magnification. The goniometer is controlled manually using differential micrometers in marked increments of 1 μm, which give corresponding angular deflections of 24 μrad/μm in the vertical direction and 35 μrad/μm in the horizontal direction.

The output of our Tsunami Ti:sapphire laser produces an elliptical and astigmatic beam, which we correct using a system of cylindrical and spherical lenses; two orthogonally oriented cylindrical lenses are used with focal lengths of 30 and 40 cm, placed 85 cm from a 600 m spherical lens. The 600 m spherical lens is 25 cm from a 2 m spherical lens, which is 2.3 m from the back focal plane of the final microscope objective at zero time delay. The optics are chosen so that a beam waist occurs at the center of the delay stage movement with Rayleigh range of ~4 m (the laser is delayed with a range of +/−0.65 m relative to this midpoint). Thus, the spot on the back focal plane of the microscope objective is well within the Rayleigh range for all time delays, and the final spot is well modeled by a Gaussian with the ratio of the major and minor axes of being $w_{0,x}/w_{0,y} \approx 1.04$, measured using a knife-edge. For all experimental data presented, the pumping and sensing spot sizes are equal.

B. One-dimensional transport

Heat transport in TDTR experiments is often nearly one-dimensional since the spot size is usually much larger than the in-plane diffusion distance. Figure 2 compares the effect of beam-offset on the measured ratio in the case of aluminum deposited on thermally-grown silicon dioxide (75 nm Al/2 μm SiO$_2$/Si) for two different spot sizes (25 μm and 4.9 μm 1/e^2 radii) with the modulation frequency fixed at $f = 9.8$ MHz. The highest thermal diffusivity in the system is for aluminum, where maximum thermal diffusion distance is $L_d \sim O([\kappa/(Cf)]^{1/2}) \approx 3$ μm, where κ is the thermal conductivity and C is the volumetric specific heat). In Figure 2(a), the spot size is much larger than the diffusion distance, and thus in-plane transport is negligible. In this case, the changes in ratio with beam offset distance x_0 are negligible.

This is, in fact, a general feature of systems with negligible in-plane transport. The dashed lines in Figure 2 show
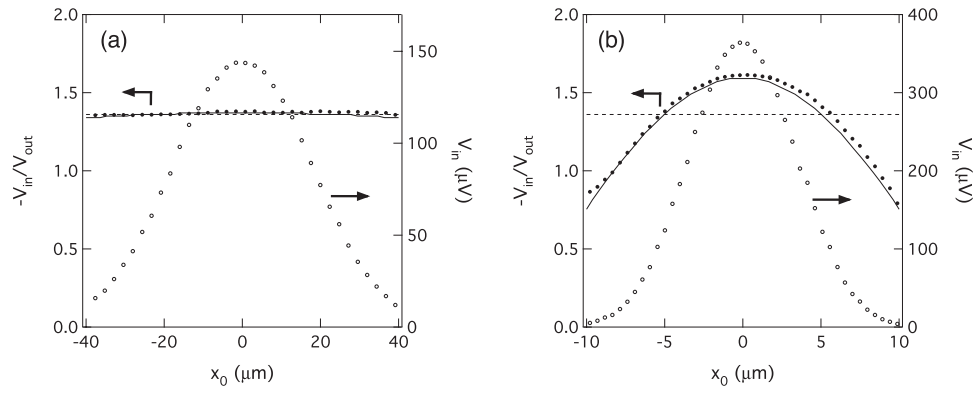
FIG. 2. Simulated and experimental signal (solid circles) for a 75 nm Al/2 μm SiO$_2$/Si sample probed using offset beams at a modulation frequency of 9.8 MHz for $1/e^2$ radii of (a) 25 μm and (b) 4.9 μm. The solid line is the simulated data for the materials stack with the in-plane thermal conductivity of aluminum taken as 175 W/m K and all anisotropic ratios taken as 1. The dashed line is the same, but assumes in-plane thermal conductivity/anisotropic ratio as zero for all layers. The right axis shows the magnitude of the in-phase signal, V_{in} (open circles).

that if the in-plane thermal conductivity is set to zero, the ratio is independent of x_0; this occurs because the temperature response function, $G(f, k)$, is exactly independent of k in the absence of in-plane thermal conduction, and can be moved outside the integral in Eq. (3). In that case, the in-phase and out-of-phase TDTR signals become

$$\text{Re}[\Delta R_M(t_d)] = A_P \Omega \frac{dR}{dT} \sum_{m=-\infty}^{\infty} (G(mf_{\text{rep}} + f_{\text{mod}}) \\ + G(mf_{\text{rep}} - f_{\text{mod}})) \exp(im2\pi f_{\text{rep}}t_d), \tag{20}$$

$$\text{Im}[\Delta R_M(t_d)] = A_P \Omega \frac{dR}{dT} \sum_{m=-\infty}^{\infty} (G(mf_{\text{rep}} + f_{\text{mod}}) \\ - G(mf_{\text{rep}} - f_{\text{mod}})) \exp(im2\pi f_{\text{rep}}t_d), \tag{21}$$

where Ω is the only variable that depends on the beam offset distance and is defined as

$$\Omega = 2\pi \int_0^{\infty} S(k; x_0)P(k)k \, dk. \tag{22}$$

Due to Ω's appearance as a prefactor, the dependence of the TDTR signal on the offset distance, x_0, vanishes upon taking the ratio in the limit of one-dimensional transport. Thus, any inflection in the ratio with beam offset distance is caused by in-plane heat transport. If the sample is measured using a spot size comparable or smaller than the in-plane diffusion distance (Figure 2(b)), then bowing in the ratio will be visible and the measurement will have sensitivity to in-plane thermal conductivity.

The presence of Ω as a prefactor to the in-phase TDTR signal allows a convenient method of determining the spot size precisely; for Gaussian beams of equal size, w_0, the in-phase signal scales like $V_{in} \sim \Omega \sim \exp(-x_0^2/w_0^2)$ when in-plane heat transport is unimportant. The in-phase signals at short positive delay time are primarily determined by the high frequency components[2] of Eq. (1), which are not affected by in-plane transport because of the short associated penetration depth. Thus, by fitting the in-phase signal at short time delay as a function of beam offset, the spot size can be measured. Spot sizes in the current paper have been measured by this method.

Although we do not individually analyze the amplitude of the in-phase or out-of-phase signals, only the ratio, it is important to point out that the magnitude of the individual signals decreases significantly with beam offset (right axis, Figure 2), and that electronic noise ultimately limits the maximum offset that can be used in the measurement. For samples with insignificant in-plane transport, the magnitude of the thermoreflectance signal scales as $V \sim \exp(-x_0^2/w_0^2)$ so that for $x_0/w_0 = 2$ the signal amplitude is only 2% of the concentrically-aligned value. On our system, we find that electronic noise floor is V_{in}, $V_{out} \lesssim 100$ nV$_{\text{rms}}$ at 9.8 MHz for the lockin-amplifier settings used here, which limits maximum beam offset. Thus, in Figure 2(b), the signal-to-noise ratio for V_{in} is 10 times larger than the noise for offsets smaller than $x_0/w_0 \approx 2.4$.

The above results show that data obtained using TDTR are insensitive to accidental non-concentric alignment of the beams. For TDTR experiments, it is generally feasible to concentrically align the beams with an offset $x_0 \leq 0.1w_0$ by maximizing the in-phase signal just after zero time delay. When in-plane heat transport is negligible, this misalignment does not affect the ratio (Figure 2(a)), and thus, does not affect the parameters extracted using TDTR. Even when in-plane transport is important, misalignment of this magnitude usually does not significantly affect the measurement. Using the example in Figure 2(b), if an accidental misalignment of $x_0/w_0 = 0.1$ is used to collect a TDTR scan (ratio vs. time delay), then the measured ratio would be only 0.2% lower than with perfectly concentric alignment. This is negligible compared to the other uncertainties in TDTR experiments.[4]

C. Measuring in-plane properties using offset beams

In Subsection III B, we showed that in-plane transport is the cause of the change in ratio with beam offset. For samples where in-plane diffusion lengths are comparable to or greater than the laser spot size, it is possible to analyze dependence

of the ratio as a function beam offset, x_0, and extract the in-plane thermal properties of materials. In this section, we provide examples of how this can be applied to anisotropic bulk materials and thin film metallic layers.

One important consideration for performing such measurements is that several parameters contribute to the signal in a beam offset sweep. Although the characteristic shape of a beam offset sweep is always caused by in-plane heat spreading, factors such as through-plane thermal conductivity and spot size are also important. For example, low through-plane thermal conductivity can enhance the in-plane spreading of heat. To determine the interdependence of parameters while extracting data, we use a type of contour plot to characterize the similarity of various fits between the experiment and model. Using the theoretical model in Sec. I, we generate the beam offset sweep curve for a given "exact" set of material properties, $r(x_0; \kappa_\perp^{exact}, \kappa_\parallel^{exact})$; here, we have written the in-plane and through-plane thermal conductivity as the parameters, for illustrative purposes. Then, we generate model curves using alternative parameters $r(x_0; \kappa_\perp, \kappa_\parallel)$, and measure how close the alternative curve is to the exact curve using a normalized residual which we define as

$$Z(\kappa_\perp, \kappa_\parallel) \equiv \left(\frac{\sum\limits_{x_0} [r(x_0; \kappa_\perp^{exact}, \kappa_\parallel^{exact}) - r(x_0; \kappa_\perp, \kappa_\parallel)]^2}{\sum\limits_{x_0} r(x_0; \kappa_\perp^{exact}, \kappa_\parallel^{exact})^2} \right)^{1/2}.$$

(23)

A contour of $Z(\kappa_\perp, \kappa_\parallel)$ thus represents fits that are similar to one another in the least-squared sense. We find that our fits to data are usually better than $Z \lesssim 0.03$, thus a contour taken at $Z = 0.03$ gives the set of possible parameter values that could be extracted by fitting the data.

To demonstrate the analysis for a bulk material, we studied highly-oriented pyrolytic graphite (HOPG) purchased from SPI Supplies (Grade-2). A fresh surface was exposed using scotch tape just prior to sputtering 70 nm of Al onto the surface. Literature values for the in-plane and through-plane thermal conductivity of HOPG have a wide range ($\kappa_\perp = 5 - 11$ W/m K and $\kappa_\parallel = 1500 - 2500$ W/m K).[10] Figure 3 shows experimental data and model fits obtained using a 10.3 μm spot size and modulation frequency of 1.6 MHz. Data were collected at two different time delays, $t_d = +300$ ps, chosen to minimize sensitivity to the thermal interface conductance, and $t_d = -300$ ps to explore the effect at negative time delay. The contour plot in Figure 4 shows that under these conditions, if there is no knowledge of the through-plane thermal conductivity, many equivalent fits are possible for the in-plane thermal conductivity ranging from $\kappa_\parallel = 1500$ to 2700 W/m K. To obtain higher accuracy, a separate measurement that is optimized to determine the through-plane thermal conductivity is beneficial. In this case, we performed a TDTR scan using a larger spot size at high modulation frequency ($w_0 = 25$ μm, 9.8 MHz) to independently obtain $\kappa_\perp = 5.4 \pm 0.7$ W/m K and the thermal conductance of the sputtered Al/graphite interface $G = 73 \pm 5$ MW/m^2 K; these are in reasonable agreement with previously reported values obtained by conventional TDTR; for Al/graphite interfaces, Schmidt has extracted $\kappa_\perp = 6.1$ W/m K and $G = 50$ MW/m^2 K; the thermal
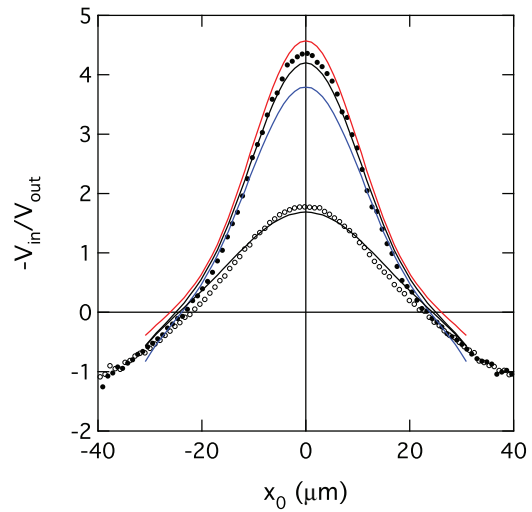

FIG. 3. Beam offset measurement of the in-plane thermal conductivity of HOPG at $f = 1.6$ MHz, $w_0 = 10.3$ μm, and $t_d = +300$ ps (solid circles). The open circles show the signal at $t = -300$ ps. The red and blue curves represent the model prediction for 20% above and below the best fit in-plane thermal conductivity ($k_\parallel = 1800$ W/m K), respectively. Through-plane thermal conductivity and thermal interface conductance were fixed at $\kappa_\perp = 5.4$ W/m K and $G = 73$ MW/m^2 K.

interface conductances for a range of electron beam evaporated metal/graphite interfaces have also been reported and generally fall in the range between 30 and 120 MW/m K near room temperature;[11] in particular, the thermal interface conductance for evaporated Al-graphite was reported as $G = 48$ MW/m^2 K at 260 K. Using the independently obtained values of $k_\perp$ and G, the beam offset sweep in Figure 3 can be fit for the in-plane heat conduction giving $\kappa_\parallel = 1800$ W/m K.

Figure 3 also shows the experimental data and model curve of the beam sweep at negative time-delay at the same location on the sample and using the same model
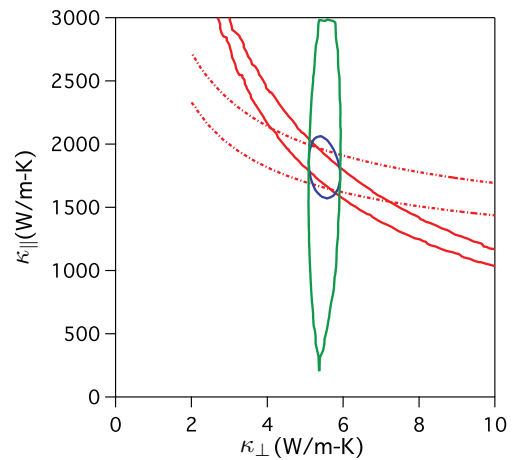

FIG. 4. Sensitivity contour map showing the interrelationship of the in-plane thermal conductivity and through-plane thermal conductivity of HOPG for beam offset sweeps conducted under different conditions. Curves are for: $f = 9.8$ MHz/$w_0 = 25$ μm (green), $f = 9.8$ MHz/ $w_0 = 10.3$ μm (blue), $f = 1.6$ MHz/ $w_0 = 10.3$ μm (red). Solid curves are at $t_d = +300$ ps, and the dashed-dotted curve is for $t_d = -300$ ps.

parameters. According to the results of the sensitivity contour (Figure 4), the accuracy obtained by fitting to data at negative time delay is not significantly different than at positive time delay. Note that at large beam offsets, the data for positive and negative time delay converge (Figure 3). Cahill has previously pointed out that for concentrically-aligned beams, the out-of-phase signal, as calculated from Eq. (2), is dominated by the lowest frequency term.[2] By contrast, the change in the in-phase signal across zero time delay represents the instantaneous temperature rise of the sample due to the pulse heating. The convergence of the beam offset signals for large offset can be understood as a limitation of the diffusion distance of the pulse heating. Once the beam offset is greater than the spot size, the ability of the sensing beam to detect the pulse heating declines and the in-phase signal detected becomes dominated by the lowest frequency term in Eq. (1) because the lowest frequency term has the largest diffusion distance.

Through judicious choice of spot-size and modulation frequency, it is sometimes possible to determine both the in-plane and through-plane properties using a single beam sweep. The contours in Figure 4 indicate that by performing the experiment using $w_0 = 10$ μm and $f = 9.8$ MHz, a simultaneous fit can be achieved. The simultaneous best fit under these conditions is shown in Figure 5, and produces similar extracted values: $\kappa_\parallel = 2100$ W/m K, $\kappa_\perp = 5.1$ W/m K.

Beam offset sweeps can also be used to measure the in-plane thermal conductivity of thin metallic layers. Figure 6 shows the measurement of a sample consisting of 24 nm Al deposited onto 500 nm thermal SiO₂/Si substrate. The Al film was deposited by magnetron sputtering at 75 W,

FIG. 6. Beam offset measurement of the in-plane thermal conductivity for a 24 nm Al film deposited onto a 500 nm layer of thermal SiO₂ /Si substrate using $f = 1.6$ MHz, $w_0 = 2.5$ μm, and $t = 1000$ ps. The red and blue curves represent the model prediction for 20% above and below the best fit ($k_\parallel = 120$ W/m K), respectively.

1 mTorr Ar (3×10^{-8} Torr base pressure) from a 1.5 in. target (99.999% pure) for 30 seconds onto a piranha cleaned substrate. By using a small spot size (2.5 μm) and a thermally insulating barrier, the effect of beam offset on the ratio is strong which allows the measurement of the in-plane properties. Similar to the case of bulk materials, the through-plane thermal conductivity of the insulating layer must be known well in order to measure the in-plane thermal conductivity of thin metal layers (Figure 7); this poses no issue since the properties of thermal SiO₂ are well known, but for other choices of substrate, an additional measurement may be required to independently measure the thermal properties
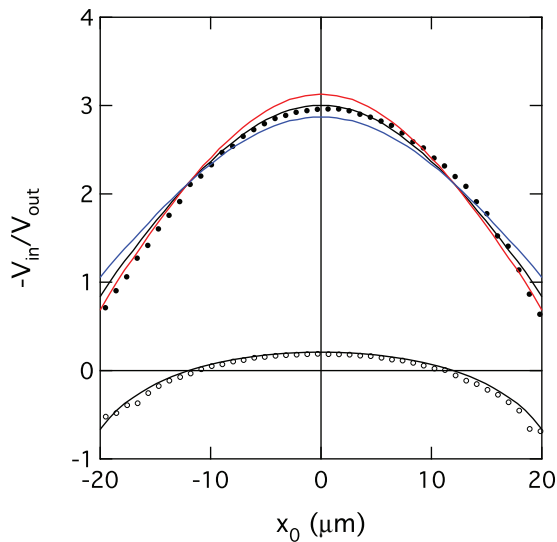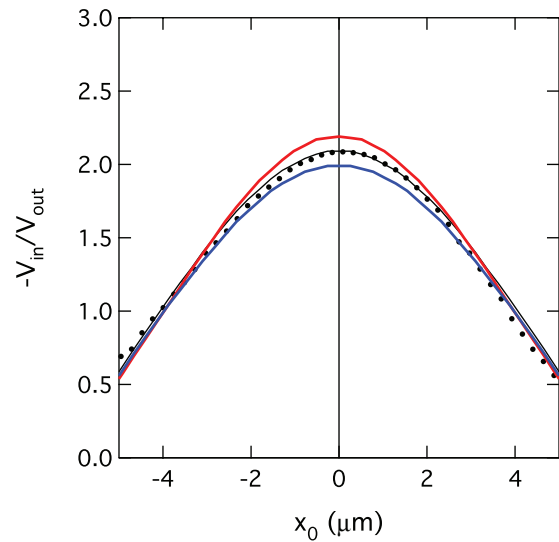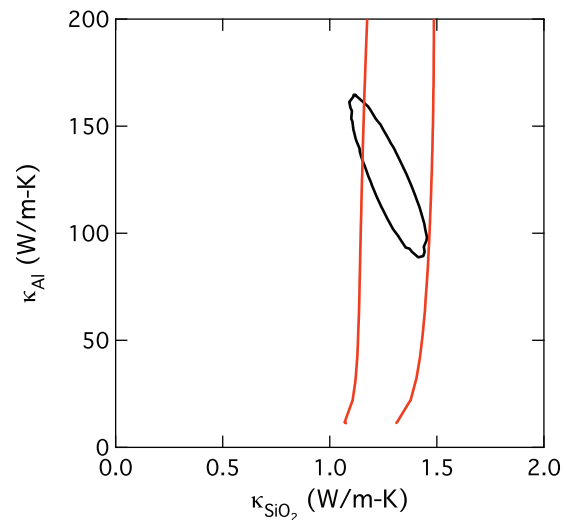

FIG. 5. Simultaneous beam offset measurement of the in-plane thermal conductivity and through-plane thermal conductivity of HOPG at $f = 9.8$ MHz, $w_0 = 10.3$ μm, and $t_d = +300$ ps (solid circles). The open circles show the signal at $t = -300$ ps. The red and blue curves represent the model prediction for 20% above and below the best fit in-plane thermal conductivity, respectively. The data are not fit to the negative time delay data, but the simulated curve for the same conditions are shown, for reference. The simultaneous best fit was for $k_\parallel = 2100$ W/m K and $k_\perp = 5.1$ W/m K. Interface conductance was fixed at $G = 73$ MW/m² K.

FIG. 7. Sensitivity contour for a beam offset measurement of thermal conductivity of 24 nm Al film deposited onto a 500 nm layer of thermal SiO₂/Si substrate. The contours are simulated for $f = 1.6$ MHz, $w_0 = 2.5$ μm, and $t = 1000$ ps (black line) and $f = 9.8$ MHz, $w_0 = 10.3$ μm, and $t = 1000$ ps (red line). The "exact" solution in Eq. (23) is taken as $\kappa_{SiO_2} = 1.3$ (W/m K), $\kappa_{Al} = 120$ (W/m K).

of the substrate. In the current example, the value extracted from the beam offset sweep (120 W/m K) matches well with the electronic thermal conductivity obtained from a 4-point probe measurement and application of the Wiedemann-Franz law (132 W/m K). The thermal conductivity is lower than our typical sputtered 70 nm Al thin films (150–200 W/m K) and bulk materials (240 W/m K), but is significantly higher than those reported by Schmidt obtained using frequency domain thermoreflectance.[7] The thermal conductivity and electrical resistivity of our thin aluminum film are consistent with previous electrical resistivity measurements for sputtered aluminum films of similar thickness.[12] Thus, we attribute the discrepancy to differences in the growth characteristics and film quality of the metal layers.

IV. CONCLUSION

In summary, a method has been presented to simulate the time-domain thermoreflectance signal that occurs using non-concentric pump and probe beams on multilayer anisotropic materials. When in-plane heat transport is negligible, the experimental signal is the same as for the concentric case. Conversely, any change in the ratio with beam-offset is due to in-plane heat transport. This has been exploited to measure the in-plane thermal conductivity of anisotropic bulk materials and thin films.

[1] A. J. Schmidt, X. Y. Chen, and G. Chen, Rev. Sci. Instrum. **79**(11), 114902 (2008).

[2] D. G. Cahill, Rev. Sci. Instrum. **75**(12), 5119 (2004).

[3] K. Kang, Y. K. Koh, C. Chiritescu, X. Zheng, and D. G. Cahill, Rev. Sci. Instrum. **79**(11), 114901 (2008).

[4] Y. K. Koh, S. L. Singer, W. Kim, J. M. O. Zide, H. Lu, D. G. Cahill, A. Majumdar, and A. C. Gossard, J. Appl. Phys. **105**(5), 054303 (2009).

[5] Y. K. Koh, Y. Cao, D. G. Cahill, and D. Jena, Adv. Funct. Mater. **19**(4), 610 (2009).

[6] R. M. Costescu, M. A. Wall, and D. G. Cahill, Phys. Rev. B **67**(5), 054302 (2003).

[7] A. J. Schmidt, R. Cheaito, and M. Chiesa, J. Appl. Phys. **107**(2), 024908 (2010).

[8] K. Kurabayashi, M. Asheghi, M. Touzelbaev, and K. E. Goodson, J. Microelectromech Syst. **8**(2), 180 (1999).

[9] B. C. Li, L. Pottier, J. P. Roger, D. Fournier, K. Watari, and K. Hirao, J. Eur. Ceram. Soc. **19**(8), 1631 (1999).

[10] Y. S. Touloukian, *Thermal Conductivity: Nonmetallic Solids* (IFI/Plenum, New York, 1970).

[11] A. J. Schmidt, K. C. Collins, A. J. Minnich, and G. Chen, J. Appl. Phys. **107**(10),104907 (2010).

[12] W. Zhang, S. H. Brongersma, O. Richard, B. Brijs, R. Palmans, L. Froyen, and K. Maex, Microelectron. Eng. **76**(1–4), 146 (2004).